

# Geometric Phases of the Uhlmann Type for $n$ -Level Gibbsian Density Matrices

Paul B. Slater

ISBER, University of California, Santa Barbara, CA 93106-2150

e-mail: [slater@itp.ucsb.edu](mailto:slater@itp.ucsb.edu), FAX: (805) 893-7995

(October 25, 2019)

We accept the implicit challenge of A. Uhlmann in his 1994 paper, “Parallel Lifts and Holonomy along Density Operators: Computable Examples Using  $O(3)$ -Orbits,” by, in fact, computing the holonomy invariants for rotations of certain  $n$ -level Gibbsian density matrices ( $n = 2, \dots, 10$ ). From these we derive, by the tracing operation, the associated geometric phases and visibilities, which we analyze and display.

PACS Numbers 03.65.Vf, 05.30.-d, 05.70.-a

In a recent paper, Sjöqvist *et al* [1] provided “a new formalism of the geometric phase for mixed states in the experimental context of quantum interferometry”. Only in passing, did these authors note that “Uhlmann was probably the first to address the issue of mixed state holonomy, but as a purely mathematical problem”.

Interested in possible (previously uninvestigated) relationships between the work of Sjöqvist *et al* [1] and that of Uhlmann [2,3], the present author compared the two approaches in terms of two spin- $\frac{1}{2}$  scenarios [4]. In the first of these, the spin- $\frac{1}{2}$  systems undergo unitary evolution along geodesic triangles [2], while in the second the unitary evolution takes place along circular paths [3]. In [3], Uhlmann had also proposed an additional scenario, which was left unanalyzed in [4]. It involves “the Gibbsian states of the form”,

$$\rho = \frac{e^{\alpha \vec{n} \cdot \vec{J}}}{\text{trace } e^{\alpha \vec{n} \cdot \vec{J}}}, \quad (1)$$

which fill for a given value of  $\alpha$  a 2-sphere called  $\mathbf{S}_j^\alpha$  if  $\vec{n}$  runs through all directions in 3-space. Now, for the starting point of the unitary evolution, one sets  $\vec{n} = (0, 0, 1)$ , while  $\vec{n} = (0, \sin \theta, \cos \theta)$  is chosen as rotational axis. The curve of state evolution is given by

$$\phi \rightarrow U(\phi)\rho_0 U(-\phi), \quad U(\phi) = e^{-i\phi(\sin \theta J_y + \cos \theta J_z)}, \quad (2)$$

and the associated parallel lift of this curve with initial value  $\rho^{1/2}$  is

$$\phi \rightarrow U(\phi)\rho_0^{1/2}V(\phi), \quad V(\phi) = e^{i\phi\tilde{H}}, \quad (3)$$

where

$$\tilde{H} = \cos \theta J_z + a \sin \theta J_y, \quad \text{and} \quad a = \frac{1}{\cosh \frac{\alpha}{2}}. \quad (4)$$

It is possible to regard  $V(\phi)$  as a rotation with angle

$$\tilde{\phi} = \kappa\phi, \quad \kappa = \sqrt{\cos^2 \theta + a^2 \sin^2 \theta} \leq 1 \quad (5)$$

and rotation axis

$$\vec{\xi} = (0, \frac{\sin \theta}{\kappa}, \frac{a \cos \theta}{\kappa}). \quad (6)$$

The holonomy invariant can be written as

$$(-1^{2j})\rho_0^{1/2}e^{2\pi i\tilde{H}}\rho_0^{1/2} = (-1^{2j})\rho_0^{1/2}e^{2\pi i\kappa}\vec{\xi} \cdot \vec{J} \rho_0^{1/2}. \quad (7)$$

(All the preceding equations are directly adopted from [2].) We have been able to compute the trace of this invariant (7) for all  $j = \frac{1}{2}, 1, \frac{3}{2}, \dots, \frac{9}{2}$ . We plot the arguments of these traces, that is the corresponding geometric phases ( $\gamma_j$ ), in Figs. 1 - 9, and their absolute values, that is the visibilities ( $\nu_j$ ), in Figs. 10 - 18. (For  $j = \frac{1}{2}$ , the results are equivalent to the first (non-Gibbsian) set of models in [2], which was compared with the analyses of Sjöqvist *et al* [1]

in [4].) Let us note that the value  $\alpha = 0$  corresponds to the fully mixed (classical) state, while  $\alpha = \pm\infty$  correspond to pure states.

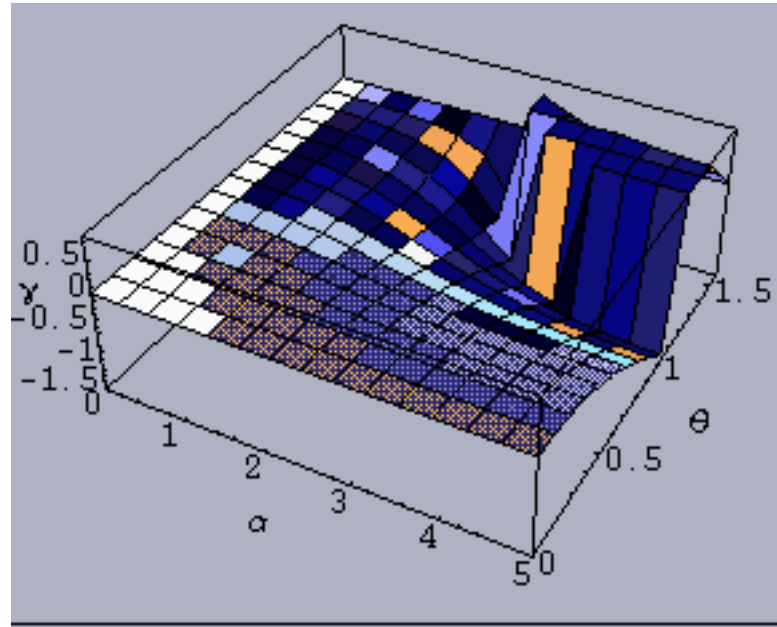


FIG. 1. Geometric phase for Gibbsian spin- $\frac{1}{2}$  systems

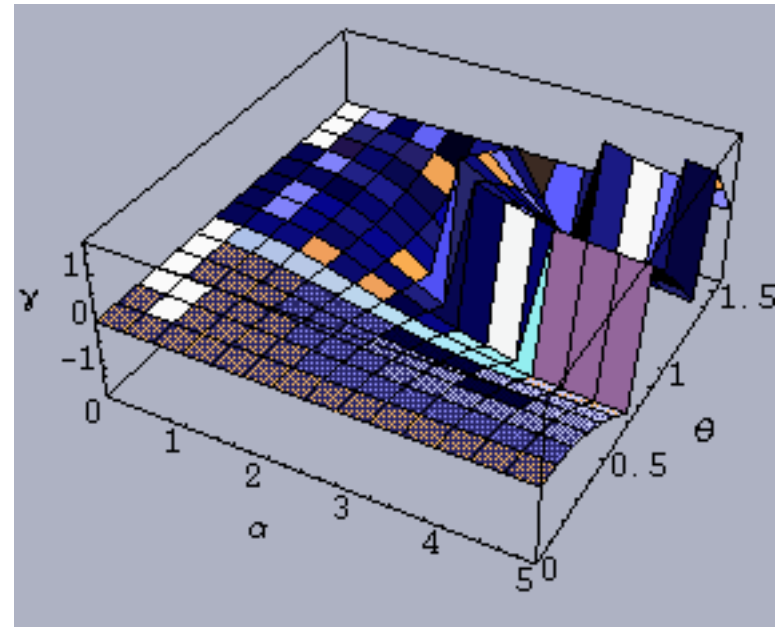


FIG. 2. Geometric phase for Gibbsian spin-1 systems

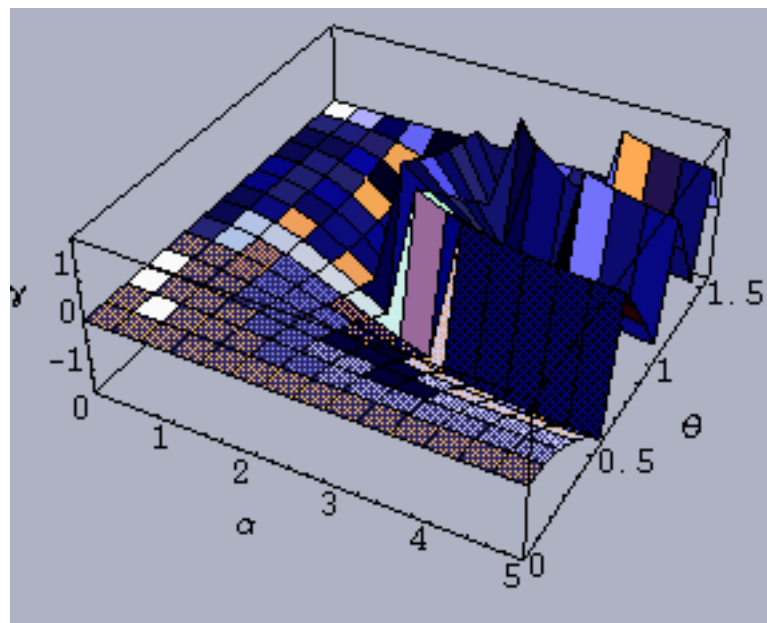


FIG. 3. Geometric phase for Gibbsian spin- $\frac{3}{2}$  systems

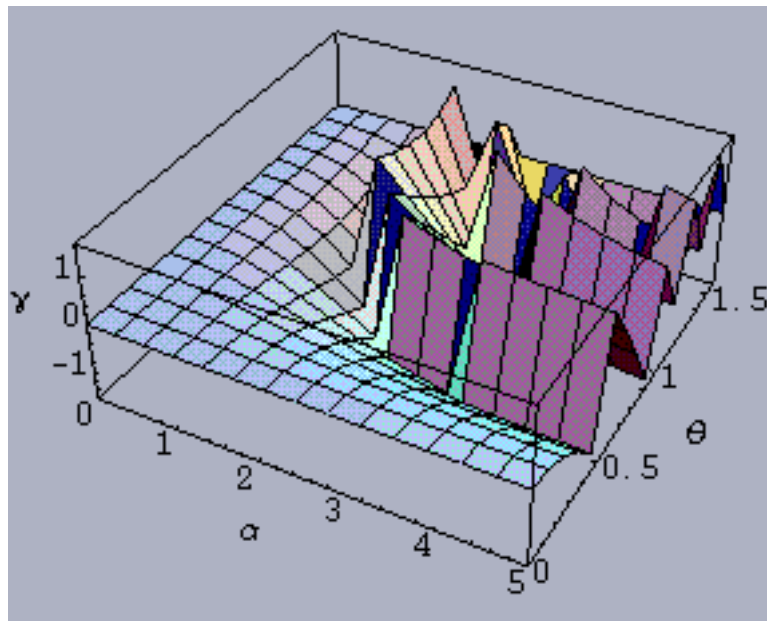


FIG. 4. Geometric phase for Gibbsian spin-2 systems

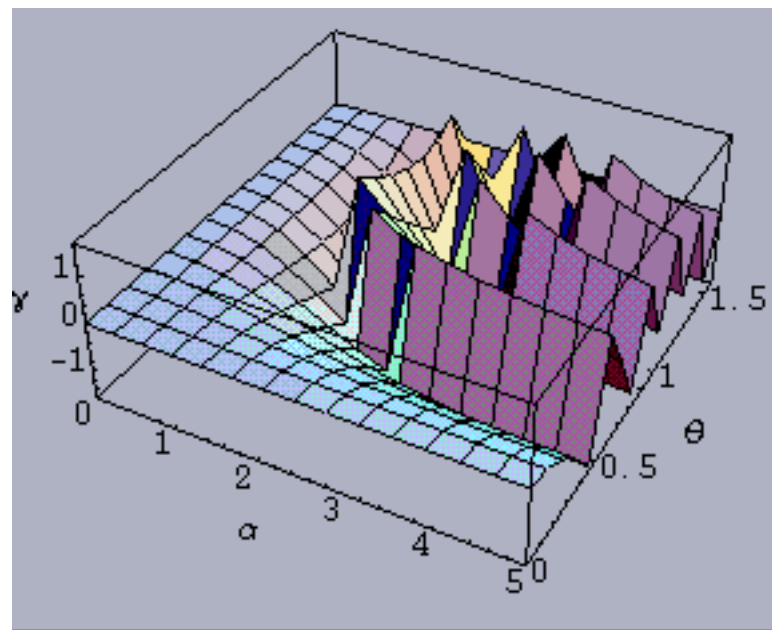


FIG. 5. Geometric phase for Gibbsian spin- $\frac{5}{2}$  systems

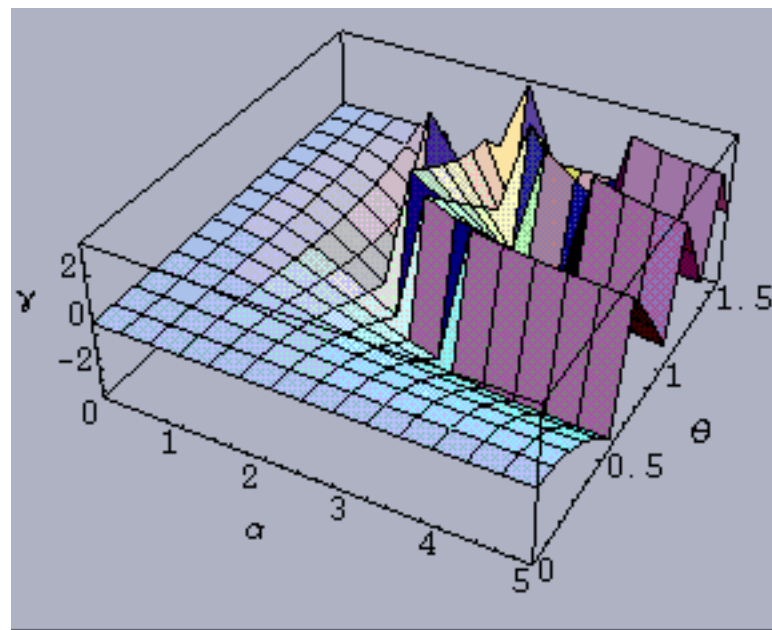


FIG. 6. Geometric phase for Gibbsian spin-3 systems

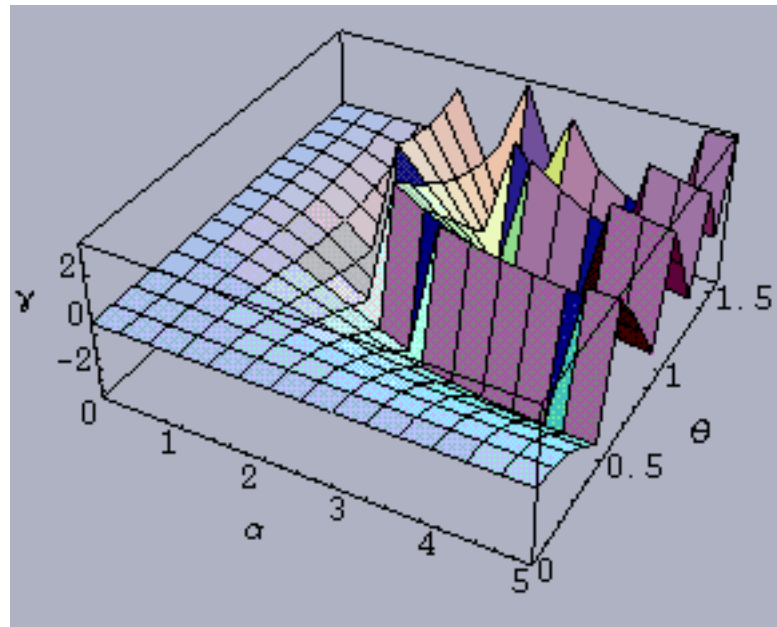


FIG. 7. Geometric phase for Gibbsian spin- $\frac{7}{2}$  systems

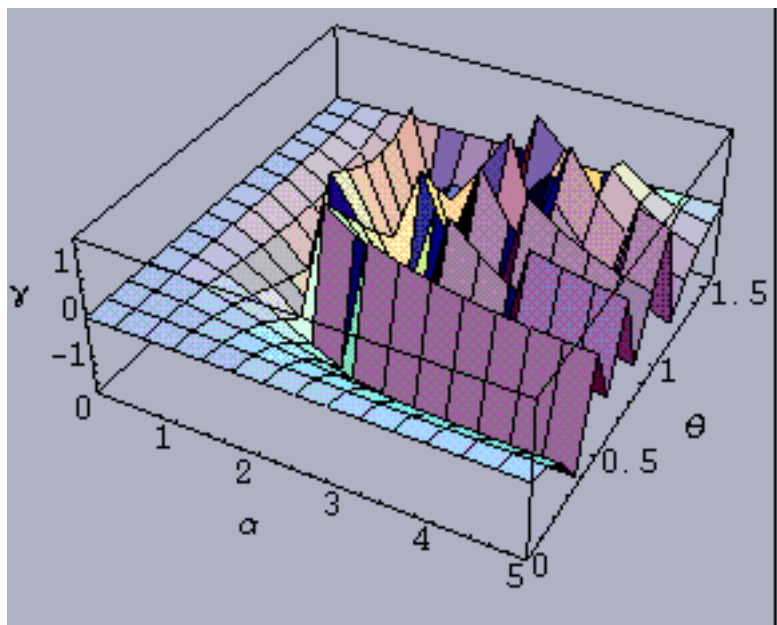


FIG. 8. Geometric phase for Gibbsian spin-4 systems

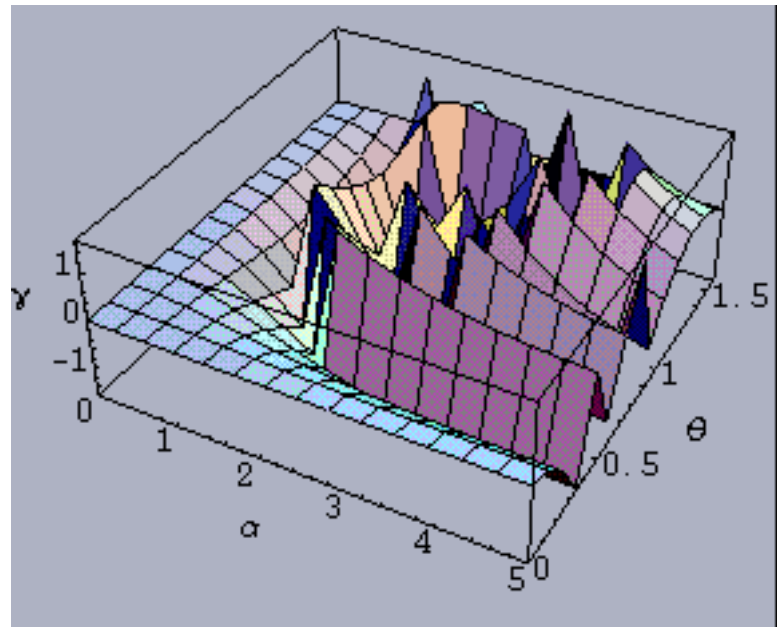


FIG. 9. Geometric phase for Gibbsian spin- $\frac{9}{2}$  systems

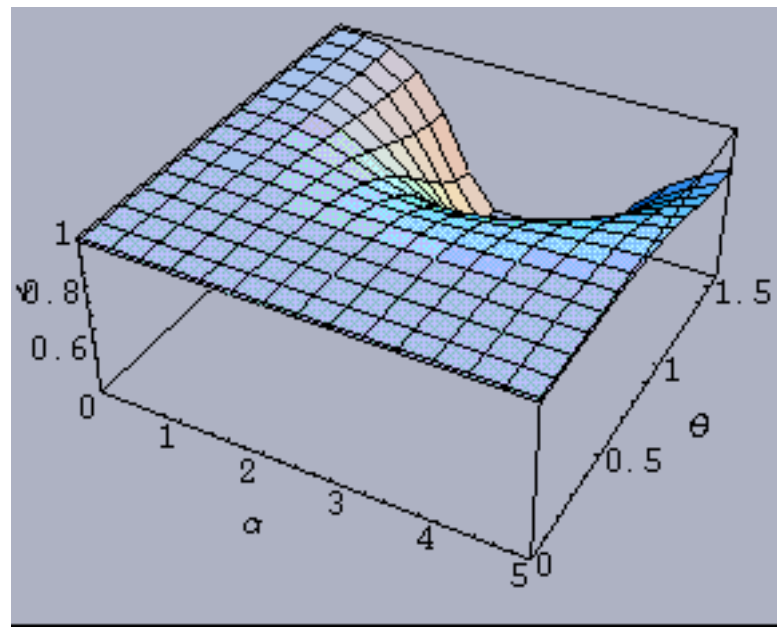


FIG. 10. Visibility for Gibbsian spin- $\frac{1}{2}$  systems

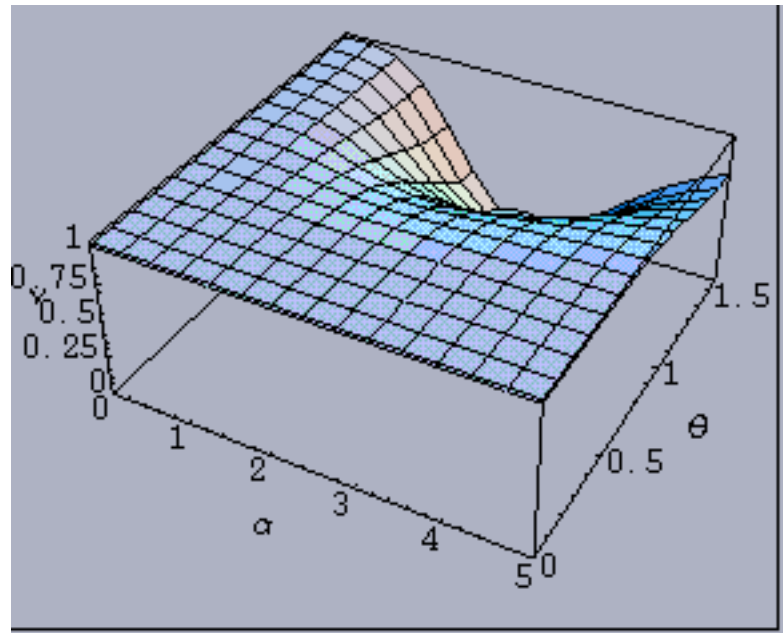


FIG. 11. Visibility for Gibbsian spin-1 systems

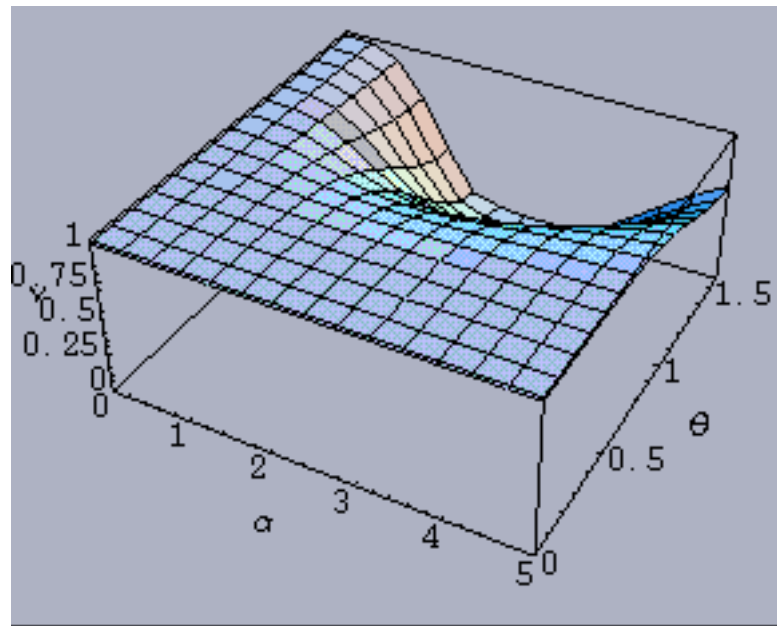


FIG. 12. Visibility for Gibbsian spin- $\frac{3}{2}$  systems

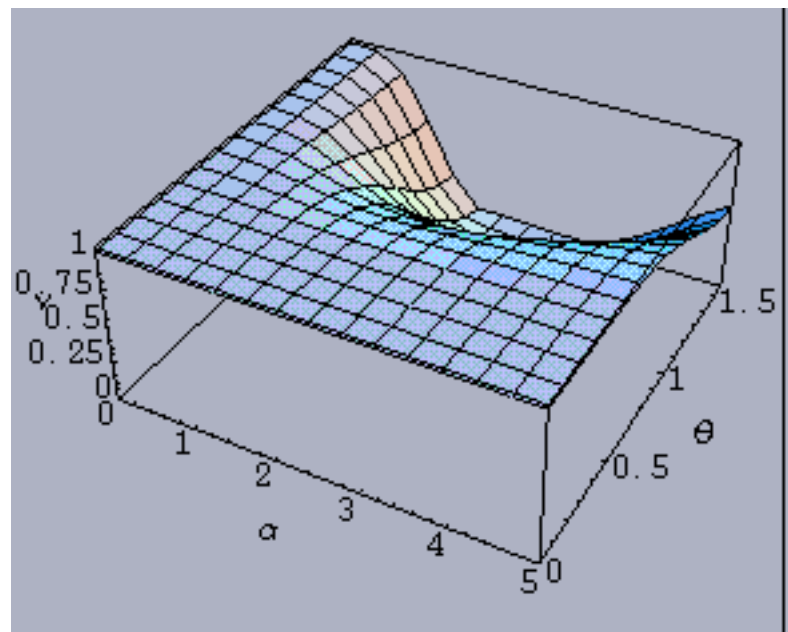


FIG. 13. Visibility for Gibbsian spin-2 systems

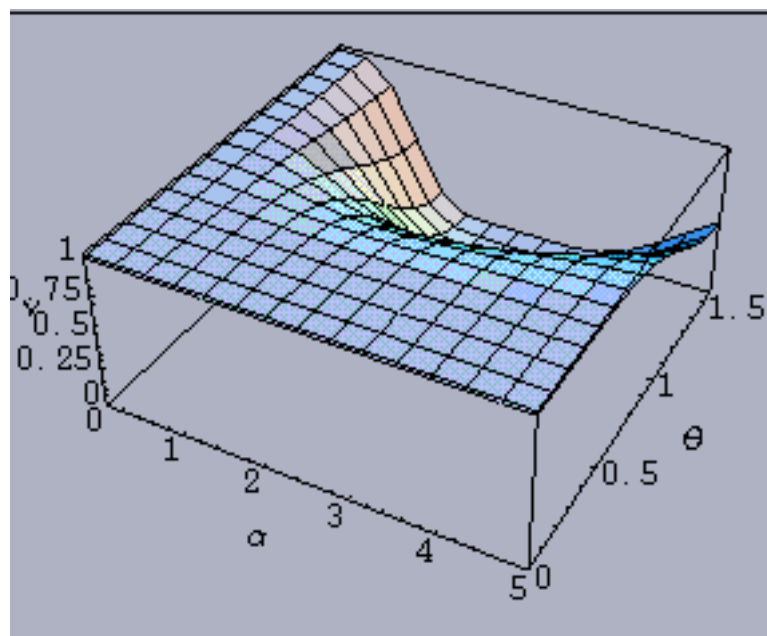


FIG. 14. Visibility for Gibbsian spin- $\frac{5}{2}$  systems

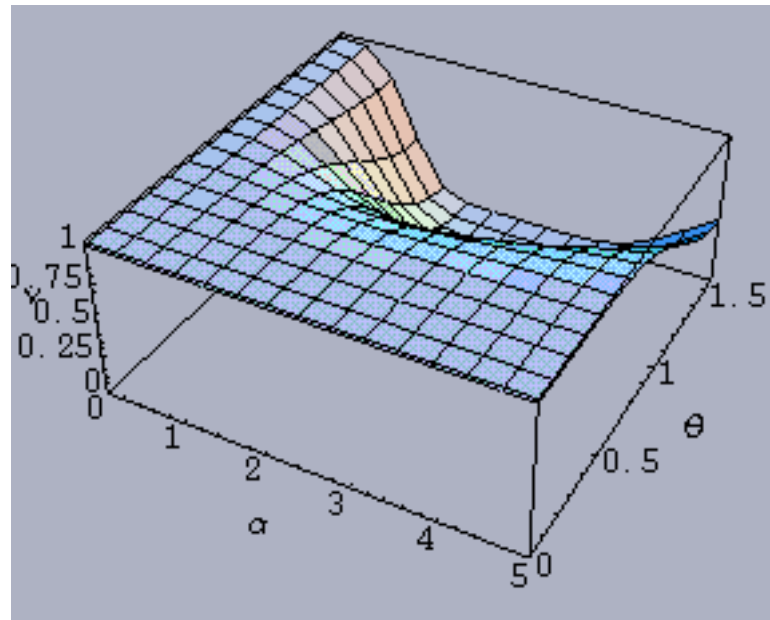


FIG. 15. Visibility for Gibbsian spin-3 systems

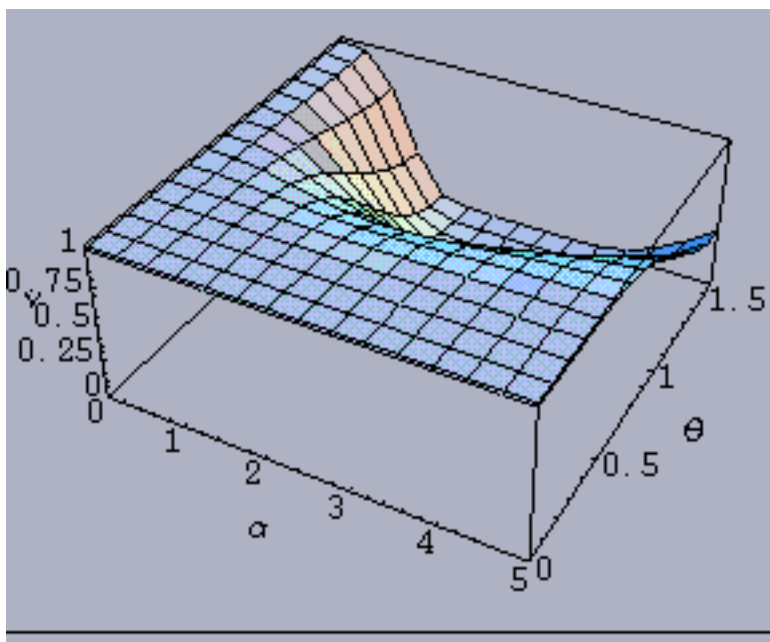


FIG. 16. Visibility for Gibbsian spin- $\frac{7}{2}$  systems

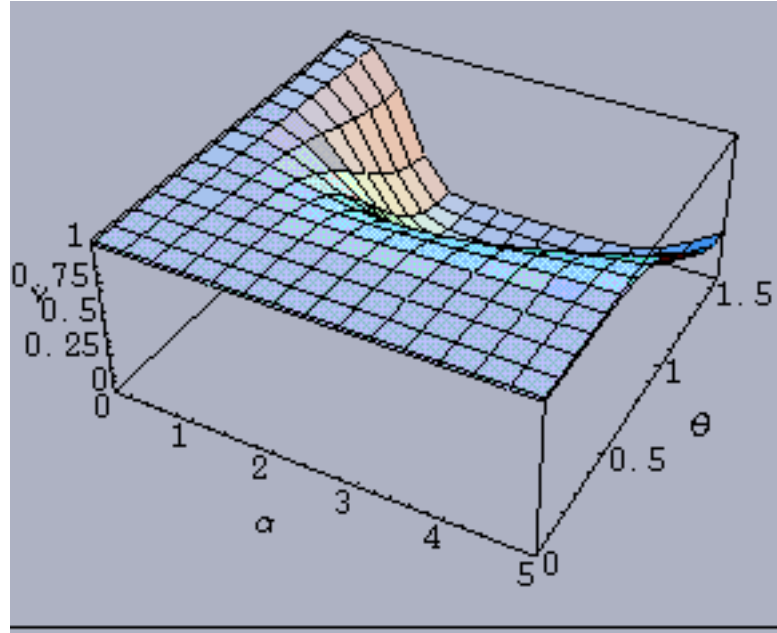


FIG. 17. Visibility for Gibbsian spin-4 systems

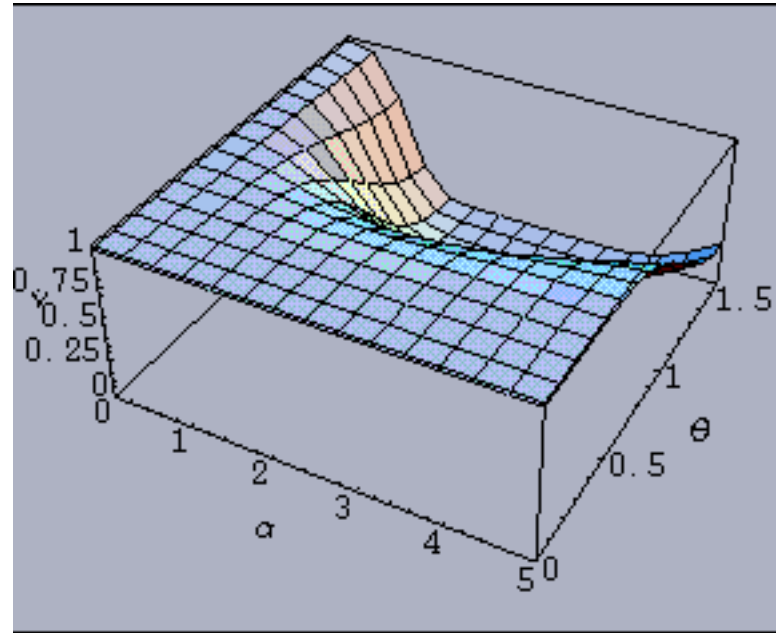


FIG. 18. Visibility for Gibbsian spin- $\frac{9}{2}$ -systems

In the spin- $\frac{1}{2}$  case (Figs. 1 and 10), we have the relations

$$\gamma_{\frac{1}{2}} = \arctan\left(\frac{2 \cos \theta \sinh \frac{\alpha}{2} \tanh i\pi\kappa}{\sqrt{\zeta}}\right), \quad (8)$$

$$\nu_{\frac{1}{2}} = \sqrt{1 - \frac{4 \sinh^2 i\pi\kappa}{\zeta}}, \quad (9)$$

where

$$\zeta = -3 + \cos 2\theta - 2 \cos^2 \theta \cosh \alpha. \quad (10)$$

One feature distinguishing the (strikingly similar) visibility plots (Figs. 10 - 18) from one another is that as  $j$  increases,  $\nu_j$  decreases at the (boundary) point  $\alpha = 5, \theta = \frac{\pi}{2}$ . For instance this value is .871618 in Fig. 10 and .498776 in Fig. 14. In Fig. 19, we plot  $\gamma_j$  ( $j = \frac{1}{2}, \dots, \frac{9}{2}$ ) versus  $\theta$ , holding  $\alpha$  fixed at 1. Curves for lower-dimensional Gibbsian systems strictly dominate those for higher-dimensional systems. (As  $\alpha$  increases, however, this simple monotonic behavior vanishes [cf. Fig. 22].)

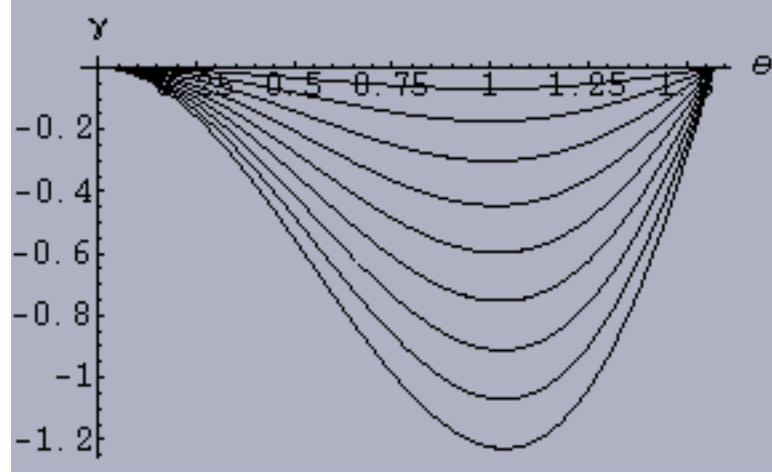


FIG. 19. Geometric phases for  $n$ -level Gibbsian systems ( $n = 2, \dots, 10$ ) holding  $\alpha = 1$ . The curve for  $n = 2$  dominates that for  $n = 3$ , which dominates that for  $n = 4, \dots$

In Fig. 20, we “reverse” this scenario, now holding  $\theta$  fixed at  $\frac{\pi}{10}$  and letting  $\alpha$  vary over  $[0,5]$ . The monotonicity of the ten curves is completely analogous to that in Fig. 19, with curves for lower  $j$  dominating those for higher  $j$ .

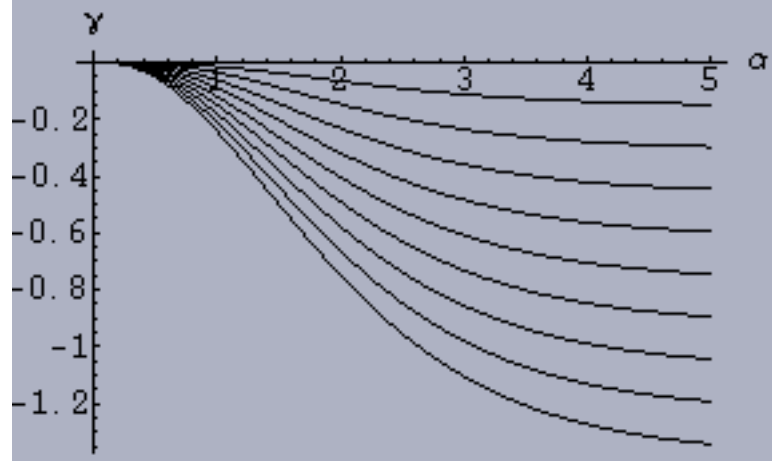


FIG. 20. Geometric phases for  $n$ -level Gibbsian systems ( $n = 2, \dots, 10$ ) holding  $\theta$  fixed at  $\frac{\pi}{10}$ . The curve for  $n = 2$  dominates that for  $n = 3$ , which dominates that for  $n = 4, \dots$

In Fig. 21, we hold  $\alpha$  at 2 and plot the *visibilities* for the ten spin scenarios. Again, as in Figs. 19 and 20, curves for lower values of  $j$  dominate those for higher values.

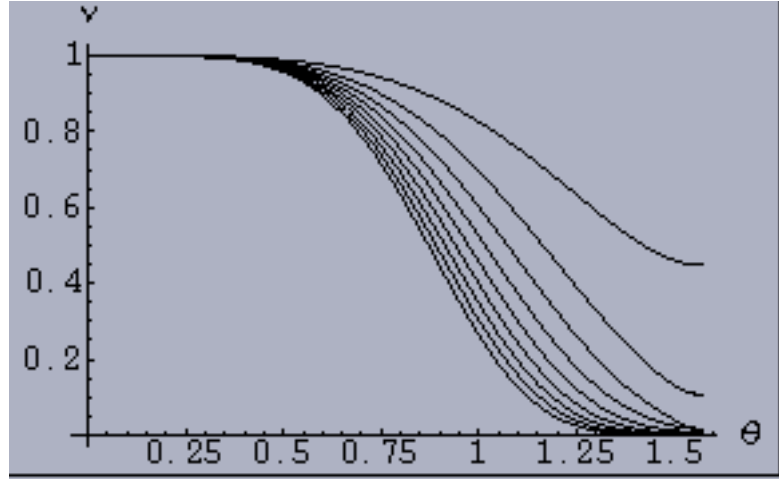


FIG. 21. Visibilities for  $n$ -level Gibbsian systems ( $n = 2, \dots, 10$ ) holding  $\alpha$  fixed at 2. The curve for  $n = 2$  dominates that for  $n = 3$ , which dominates that for  $n = 4, \dots$

While in Fig. 19  $\alpha$  was fixed at 1, in Fig. 22, it is held at 2. Now the same simple monotonicity with  $j$  observed in the preceding three figures, holds below  $\theta \approx .46$ . However, it is lost at higher values of  $\theta$ , with the curves for the higher spin states jumping from  $-\pi$  to  $\pi$  at lower values of  $\theta$  than do the curves for the lower spin states (with the exception of  $j = \frac{1}{2}$  and 1, the curves for which do not jump in this fashion).

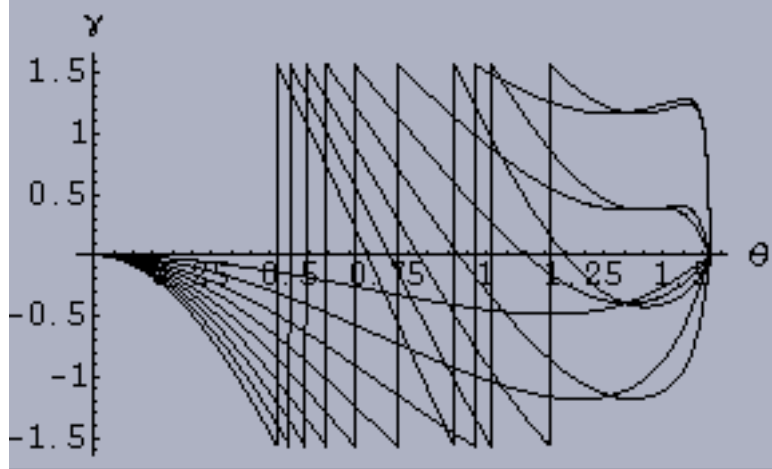


FIG. 22. Geometric phases for  $n$ -level Gibbsian systems ( $n = 2, \dots, 10$ ) holding  $\alpha = 2$ . Only below  $\theta \approx .46$  does the curve for  $n = 2$  dominate that for  $n = 3$ , which dominates that for  $n = 4, \dots$

In Fig. 23, in which  $\theta$  is fixed at  $\frac{\pi}{5}$ , similar behavior to that observed in Fig. 22 takes place. Below  $\alpha \approx 1.43$ , the simple monotonicity with  $j$  holds, then the curves begin to jump from  $-\pi$  to  $\pi$  with the curves for higher  $j$  jumping first.

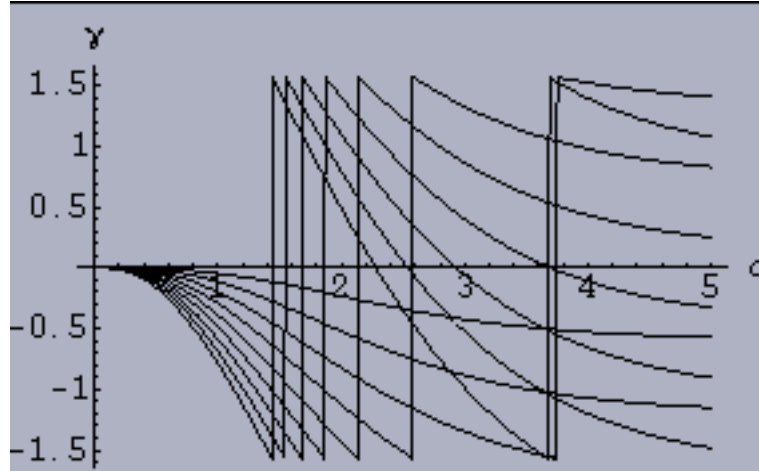


FIG. 23. Geometric phases for  $n$ -level Gibbsian systems ( $n = 2, \dots, 10$ ) holding  $\theta = \frac{\pi}{5}$ . Only below  $\alpha \approx 1.43$  does the curve for  $n = 2$  dominate that for  $n = 3$ , which dominates that for  $n = 4, \dots$

In Fig. 24, holding  $\theta = \frac{\pi}{2}$ , we plot the various visibilities over the range  $\alpha \in [1, 4]$ . At  $\alpha = 2.2$ , the values of  $\nu_j$  monotonically decline from  $j = \frac{1}{2}$  to  $\frac{9}{2}$ .

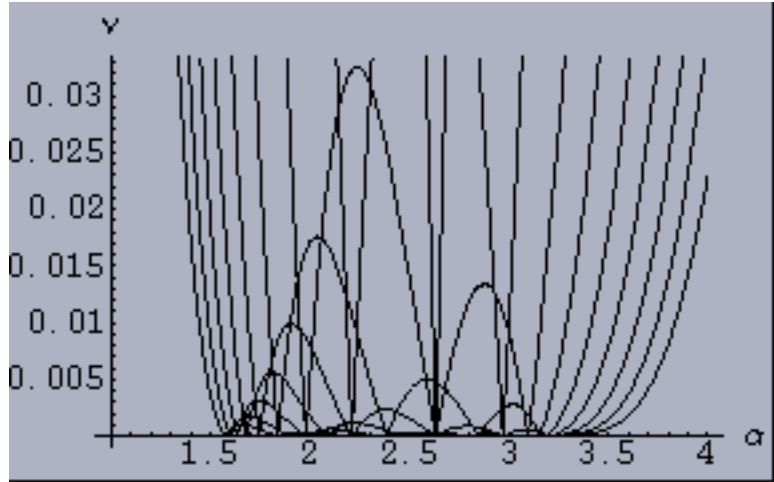


FIG. 24. Visibilities for  $n$ -level Gibbsian systems ( $n = 2, \dots, 10$ ) fixing  $\theta = \frac{\pi}{2}$ . At  $\alpha = 2.2$ , the values of  $\nu$  monotonically decline as  $n$  increases. The highest peak belongs to  $n = 2$ .

#### ACKNOWLEDGMENTS

I would like to express appreciation to the Institute for Theoretical Physics for computational support in this research.

---

[1] E. Sjöqvist, A. K. Pati, A. Ekert, J. S. Anandan, M. Ericsson, D. K. L. Oi and V. Vedral, Phys. Rev. Lett. 85, 2845 (2000).  
[2] A. Uhlmann, in Nonlinear, Dissipative, Irreversible Quantum Systems, edited by H.-D. Doebner, V. K. Dobrev and P. Nattermann, (Clausthal, 1994).  
[3] A. Uhlmann, in *Symmetries in Science VI*, edited by B. Gruber, (Plenum, New York, 1993), p. 741.  
[4] P. B. Slater, e-print, math-ph/0111014.